2014 IEEE International Conference on Robotics & Automation (ICRA)
Hong Kong Convention and Exhibition Center
May 31 - June 7, 2014. Hong Kong, China

# Universal Balancing Controller for Robust Lateral Stabilization of Bipedal Robots in Dynamic, Unstable Environments

Umashankar Nagarajan and Katsu Yamane

*Abstract*— **This paper presents a novel universal balancing controller that successfully stabilizes a planar bipedal robot in dynamic, unstable environments like seesaw and bongoboards, and also in static environments like curved and flat floors. These different dynamic systems have state spaces with different dimensions, and hence instead of using full state feedback, the universal controller is derived as a single output feedback controller that stabilizes them. This paper analyzes the robustness of the derived universal controller to disturbances and parameter uncertainties, and demonstrates its universality and superiority to similarly derived LQR and $H_\infty$ controllers. This paper also presents nonlinear simulation results of the universal controller successfully stabilizing a family of bongoboard, curved floor, seesaw, tilting and rocking floor models.**

## I. Introduction

Dynamic balancing of bipedal robots is one of the most fundamental and challenging problems in robotics with a large body of work on postural stabilization [1], [2], push recovery [3], [4] and walking [5], [6]. Bipedal robots can exploit the passive dynamics of their legs to balance in the sagittal plane, but significant active control is essential for balancing in the coronal (lateral) plane [7]. This paper presents a universal lateral balancing controller for bipedal robots that successfully balances in dynamic, unstable environments like seesaw and bongoboards, and also in static environments like flat and curved floors as shown in Fig. 1.

Balancing controllers for simplified models derived based on the balance recovery strategies of humans while balancing on slacklines and tightropes were presented in [8], [9]. Momentum based control strategies that actively control the ground reaction forces on each foot to successfully stabilize humanoid robots on non-level and rocking floors were presented in [10]. However, unstable environments like seesaw and bongoboards were not considered. Several researchers have explored control strategies for enabling bipedal robots to walk on a rolling ball [11], balance on a bongoboard [12] and on a seesaw [13]. However, all these approaches dealt with designing different full state feedback controllers for balancing in different dynamic environments.

This paper derives a first of its kind universal balancing controller as an output feedback controller that successfully stabilizes planar bipedal robots in dynamic, unstable environments like seesaw and bongoboards, and also in static environments like flat and curved floors. To the best of our knowledge, this is the first approach wherein a single controller stabilizes different dynamic systems with state spaces of different dimensions. This paper demonstrates the universality and superiority of the derived universal controller over similarly derived LQR and $H_\infty$ controllers in terms of robustness to disturbances and parameter uncertainties. It also presents nonlinear simulation results of the universal controller successfully stabilizing a family of bongoboard, seesaw, curved floor, tilting and rocking floor models.

U. Nagarajan and K. Yamane are with Disney Research Pittsburgh, PA, 15213 USA umashankar@disneyresearch.com, kyamane@disneyresearch.com

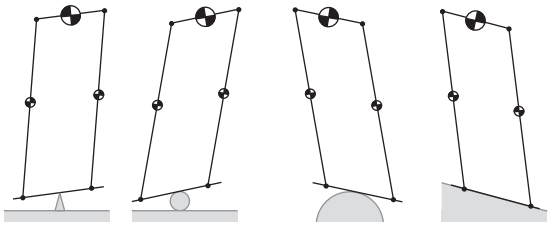

(*a*) (*b*) (*c*) (*d*)

Fig. 1: Planar bipedal robot modeled as a four-bar linkage balancing in different static and dynamic, unstable environments: (*a*) Seesaw, (*b*) Bongoboard, (*c*) Curved floor, and (*d*) Non-level flat floor.

## II. Background: Static Output Feedback Control

The universal controller presented in this paper is formulated as a static output feedback controller [14], [15], and this section briefly describes an iterative algorithm from [16] used in this paper to derive output feedback controllers.

Consider a continuous time-invariant linear system

$$\begin{aligned} \dot{x} &= Ax + Bu, \\ y &= Cx, \end{aligned} \tag{1}$$

where $x \in \mathbb{R}^{n\times 1}$ is the state vector, $u \in \mathbb{R}^{m\times 1}$ is the control input vector, and $y \in \mathbb{R}^{p\times 1}$ is the output vector with $p < n$ and rank($C$) = $p$. The goal of static output feedback control is to find a time-invariant output feedback gain $F \in \mathbb{R}^{m\times p}$ such that $u = -Fy$ stabilizes the system in Eq. 1. Given an output feedback gain $F$, its resulting state feedback gain is given by $K = FC \in \mathbb{R}^{m\times n}$. Alternatively, given a state feedback gain $K$, the output feedback gain is derived as

$$F = KC^\dagger, \tag{2}$$

where $C^\dagger \in \mathbb{R}^{n\times p}$ is the Moore-Penrose pseudoinverse of the output matrix $C \in \mathbb{R}^{p\times n}$. It is important to note that not all stabilizing state feedback gains $K$ result in stabilizing output feedback gains $F$ given by Eq. 2.

The singular value decomposition of the output matrix $C$ gives $C = USV^T$, where $U \in \mathbb{R}^{p\times p}$, $V \in \mathbb{R}^{n\times n}$ are unitary matrices, and $S \in \mathbb{R}^{p\times n}$ is a rectangular diagonal matrix containing the singular values of $C$. Moreover, $V = [V_1, V_2]$, where $V_1 \in \mathbb{R}^{n\times p}$ and $V_2 \in \mathbb{R}^{n\times(n-p)}$. Using this, the static

output feedback stabilization problem can be formulated as the following constrained optimization problem of finding a state feedback gain $K$:

$$\begin{aligned} \underset{K}{\text{minimize}} \quad & E\left[\int_0^\infty \left(x^T Q x + u^T R u\right) dt\right], \\ \text{subject to} \quad & KV_2 = 0, \end{aligned} \tag{3}$$

where, $u = -Kx$, and $Q \in \mathbb{R}^{n\times n}$ and $R \in \mathbb{R}^{m\times m}$ are positive-semidefinite and positive-definite matrices respectively. More details on this formulation can be found in [16]. If Eq. 3 has a solution, then the optimal stabilizing state feedback gain $K$ satisfies the following conditions:

$$(A - BK)Y + Y(A - BK)^T + X = 0, \tag{4}$$

$$(A - BK)^T P + P(A - BK) + K^T R K + Q = 0, \tag{5}$$

$$K - R^{-1}B^T P\left[I - V_2\left(V_2^T Y^{-1} V_2\right)^{-1} V_2^T Y^{-1}\right] = 0, \tag{6}$$

where $X, Y, P \in \mathbb{R}^{n\times n}$ are all symmetric, positive-definite matrices. Here, $Q$, $R$ and $X$ are defined by the user. Any stabilizing state feedback gain $K$ that satisfies Eq. 4−6 produces a stabilizing output feedback gain $F$ given by Eq. 2. The proof of this statement can be found in [16].

Algorithm 1 presents the iterative convergent algorithm described in [16], which solves the constraint optimization in Eq. 3. At every iteration, the algorithm solves Lyapunov equations in Eq. 4−5, and uses Eq. 6 to update the state feedback gain such that $K_{i+1}$ in Eq. 8 stabilizes the system in Eq. 1 and as $i \to \infty$, $K_i V_2 \to 0$ producing a stabilizing output feedback gain $F_i$. The algorithm iterates until $||K_i V_2|| < \epsilon$ (Step 5), and the norm can be either $L_2$-norm or Frobenius norm. In this work, Frobenius norm is used and $\epsilon$ is chosen to be $10^{-5}$. The proof of convergence of Algorithm 1 and the bounds on $\beta_i$ that guarantee stability of the closed loop system can be found in [16].

**Algorithm 1:** Output Feedback Control (OFC) Design

**input** : System $\{A, B, C\}$, Matrices $Q, R, X$
**output** : Output Feedback Control Gain $F$
**function**: $F$ = OFC($A, B, C, Q, R, X$)

1 **begin**
2 Do singular value decomposition of $C$ and obtain $V_2$
$[U, S, V]$ = svd($C$)
$V_2 = V(:, p+1:n)$
3 Solve algebraic Riccati equation to get initial gain
$A^T N + NA - NBR^{-1}B^T N + Q = 0$
$K_0 = B^T N$ (7)
4 $i = 0$
5 **while** $||K_i V_2|| \geq \epsilon$ **do**
6 Solve Lyapunov equations to get $Y_i$ and $P_i$ (Eq. 4−5)
$(A - BK_i)Y_i + Y_i(A - BK_i)^T + X = 0$
$(A - BK_i)^T P_i + P_i(A - BK_i) + K_i^T R K_i + Q = 0$
7 Get state feedback gain increment (Eq. 6)
$K_i' = R^{-1}B^T P\left[I - V_2\left(V_2^T Y^{-1} V_2\right)^{-1} V_2^T Y^{-1}\right]$
$\Delta K_i = K_i' - K_i$
8 Update state feedback gain
$K_{i+1} = K_i + \beta_i \Delta K_i$, (8)
such that $\beta_i > 0$ and $A - BK_{i+1}$ is stable
9 $i = i + 1$
10 **end**
11 Get output feedback gain $F = K_i C^\dagger$ (Eq. 2)
12 **end**

TABLE I: Nominal System Parameters for the Bongoboard Model

| Parameter | Symbol | Value |
|---|---|---|
| Wheel Density | $\rho_w$ | 200 kg·m$^{-3}$ |
| Wheel Radius | $r_w$ | 0.1 m |
| Wheel Mass | $m_w$ | 6.28 kg |
| Wheel Moment of Inertia | $I_w$ | 0.035 kg·m$^2$ |
| Board Mass | $m_b$ | 2 kg |
| Board Moment of Inertia | $I_b$ | 0.1067 kg·m$^2$ |
| Board Length | $l_b$ | 0.8 m |
| Link-1 Mass | $m_1$ | 15 kg |
| Link-1 Moment of Inertia | $I_1$ | 1 kg·m$^2$ |
| Link-1 Length | $l_1$ | 1 m |
| Link-2 Half Mass | $m_2$ | 15 kg |
| Link-2 Half Moment of Inertia | $I_2$ | 2 kg·m$^2$ |
| Link-2 Half Length | $l_2$ | 0.1 m |

## III. Robot and Dynamic Environment Models

The work presented in this paper focuses on lateral balancing tasks, and hence the robot model is limited to the coronal plane of a bipedal robot. The planar bipedal robot is modeled as a four-bar linkage with three constraints (two position constraints and one angular constraint) at the pelvis and four actuators corresponding to ankle and hip joints.

### A. Planar Bipedal Robot on a Bongoboard

The bongoboard is modeled as a rectangular rigid board (negligible thickness) with rolling contact on top of a rigid cylindrical wheel. The planar bipedal robot is assumed to be rigidly attached to the board such that the feet cannot slide or lose contact. The bongoboard model has three degrees of freedom (DOF), one for the robot and two for the bongoboard, and its system parameters are listed in Table I. The model also assumes that there is no slip between the wheel and the board, or the wheel and the floor. Moreover, the event of the board hitting the floor is ignored.

Figure 2 shows the configurations of the robot on the bongoboard, and the configuration vector is given by $q = [\alpha_w, \alpha_b, \theta_1^l, \theta_1^r, \theta_2^l, \theta_2^r]^T \in \mathbb{R}^{6\times 1}$, where $\alpha_w$ is the configuration of the wheel, $\alpha_b$ is the configuration of the board relative to the wheel, $\theta_1^l, \theta_1^r$ are the link-1 configurations of the left and right legs respectively, and $\theta_2^l, \theta_2^r$ are the link-2 configurations of the left and right legs respectively.

The equations of motion are derived using Euler-Lagrange equations and can be written in matrix form as follows:

$$M(q)\ddot{q} + h(q, \dot{q}) = s_\tau^T \tau + \Psi(q)^T \lambda, \tag{9}$$

where $M(q) \in \mathbb{R}^{6\times 6}$ is the mass/inertia matrix, $h(q, \dot{q}) \in \mathbb{R}^{6\times 1}$ is the vector containing Coriolis, centrifugal and gravitational forces, $s_\tau = [0_{4\times 2}, I_4] \in \mathbb{R}^{4\times 6}$ is the input coupling matrix, $I_4 \in \mathbb{R}^{4\times 4}$ is the identity matrix, $\tau \in \mathbb{R}^{4\times 1}$ is the vector of actuator inputs, $\Psi(q) \in \mathbb{R}^{3\times 6}$ is the constraint

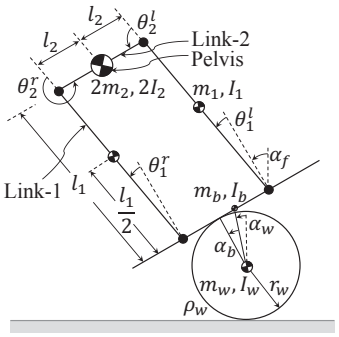


Fig. 2: Bongoboard dynamic model.

matrix, and $\lambda \in \mathbb{R}^{3\times 1}$ is the vector of constraint forces at the pelvis corresponding to two position constraints and one angular constraint. Here, the contact forces at the feet are ignored since the feet are assumed to be rigidly fixed to the board. In a real robot, this can be achieved by strapping its feet to the board like in a snowboard. The constraints given by $\Psi(q)\dot{q} = 0 \in \mathbb{R}^{3\times 1}$ are differentiated to get

$$\Psi(q)\ddot{q} + \dot{\Psi}(q,\dot{q})\dot{q} = 0 \in \mathbb{R}^{3\times 1}. \tag{10}$$

Eliminating $\lambda$ from Eq. 9−10,

$$\begin{aligned} \ddot{q} &= M^{-1}(q)\big(N_2(q)(s_\tau^T\tau - h(q,\dot{q})) - N_1(q)\dot{\Psi}(q,\dot{q})\dot{q}\big), \\ &= \Phi(q,\dot{q},\tau), \end{aligned} \tag{11}$$

where $N_1(q) = \Psi^T(q)(\Psi(q)M^{-1}(q)\Psi^T(q))^{-1}$, $N_2(q) = (I_6 - N_1(q)\Psi(q)M^{-1}(q))$, and $I_6 \in \mathbb{R}^{6\times 6}$ is the identity matrix. The linear state space matrices for the state vector $x = [q^T, \dot{q}^T]^T \in \mathbb{R}^{12\times 1}$ are:

$$\begin{aligned} A &= \left[\begin{array}{cc} 0_{6\times 6} & I_6 \\ \frac{\partial\Phi}{\partial q} & \frac{\partial\Phi}{\partial\dot{q}} \end{array}\right]\Bigg|_{x=0,\tau=0} \in \mathbb{R}^{12\times 12}, \\ B &= \left[\begin{array}{c} 0_{6\times 4} \\ \frac{\partial\Phi}{\partial\tau} \end{array}\right]\Bigg|_{x=0,\tau=0} \in \mathbb{R}^{12\times 4}. \end{aligned} \tag{12}$$

However, the pair $(A, B)$ in Eq. 12 is not controllable because its realization is not minimal. Given an output matrix $C \in \mathbb{R}^{p\times 12}$, where rank($C$) = $p$, the minimal realization $\{A_m, B_m, C_m\}$ of $\{A, B, C\}$ is given by Kalman decomposition [17], which provides an orthonormal state transformation $U_m \in \mathbb{R}^{6\times 12}$ such that $A_m = U_m A U_m^T \in \mathbb{R}^{6\times 6}$, $B_m = U_m B \in \mathbb{R}^{6\times 4}$ and $C_m = C U_m^T \in \mathbb{R}^{p\times 6}$. Here, six out of twelve states corresponding to the three constraints in Eq. 10 have been removed to obtain the minimal system.

### *B. Planar Bipedal Robot on Seesaw, Flat and Curved Floors*

The model of the planar bipedal robot on a seesaw and a board on top of a curved floor have 2-DOF, one each for the robot and the board, whereas the flat floor model has only 1-DOF. The derivation of the seesaw model is similar to that of the bongoboard model wherein the wheel configuration $\alpha_w$ is omitted, and the board is attached to the floor at its center via a hinge joint. The curved floor model is derived as a special case of the bongoboard model with large wheel radius $r_w$, mass $m_w$ and moment of inertia $I_w$, whereas the flat floor model is derived as a special case of the seesaw model with large board mass $m_b$ and moment of inertia $I_b$.

The bongoboard model can be used as a generic model wherein different wheel radii can represent the different environments discussed above. The seesaw and flat floor models correspond to two discrete cases with zero ($r_w = 0$) and infinite ($r_w = \infty$) wheel radii respectively. The range of wheel radii between zero and infinity, $i.e., r_w \in (0, \infty)$, for a bongoboard model with constant wheel density correspond to a continuum of bongoboard and curved floor models.

## IV. Universal Controller

The universal controller is a single controller that stabilizes the bongoboard, seesaw, curved floor and flat floor models with six, four, four and two minimal states respectively. Since the state space for each case is of a different dimension, the universal controller cannot be a full state feedback controller. This section proposes to design the universal controller as an output feedback controller, wherein it maps the same outputs from each case to the same control inputs of the robot.

The universal controller presented in this paper uses five outputs for feedback. The first two outputs are chosen to be the global position and velocity of the pelvis (Fig. 2) measured using the left link-1 and link-2 angles and angular velocities respectively, while the next three outputs are chosen to be the right link-1 angle, angular velocity, and the global foot angle $\alpha_f$ as shown in Fig. 2. The global foot angle $\alpha_f$ and global position and velocity of the pelvis can be estimated using an inertial measurement unit [18] at the pelvis. These outputs can be measured without direct measurements of the environment, $i.e.$, wheel angle $\alpha_w$ and board angle $\alpha_b$ relative to the wheel. The output matrix $C \in \mathbb{R}^{5\times 12}$ for the bongoboard model can be written as

$$C = \left[\begin{array}{cc} C_1 & C_2 \end{array}\right], \tag{13}$$

where,

$$C_1 = \left[\begin{array}{cccccc} -l_1-l_2-2r_w & -l_1-l_2 & -l_1-l_2 & 0 & -l_2 & 0 \\ 0 & 0 & 0 & 0 & 0 & 0 \\ 0 & 0 & 0 & 1 & 0 & 0 \\ 0 & 0 & 0 & 0 & 0 & 0 \\ 1 & 1 & 0 & 0 & 0 & 0 \end{array}\right],$$

$$C_2 = \left[\begin{array}{cccccc} 0 & 0 & 0 & 0 & 0 & 0 \\ -l_1-l_2-2r_w & -l_1-l_2 & -l_1-l_2 & 0 & -l_2 & 0 \\ 0 & 0 & 0 & 0 & 0 & 0 \\ 0 & 0 & 0 & 1 & 0 & 0 \\ 0 & 0 & 0 & 0 & 0 & 0 \end{array}\right].$$

The output matrix for the seesaw model $C \in \mathbb{R}^{5\times 10}$ can be similarly derived. Using Algorithm 1, one can verify that the bongoboard, seesaw, curved floor and flat floor models are output feedback stabilizable with these outputs. In fact, just the first three outputs are sufficient to stabilize these models.

One may wonder why five outputs were picked and not more. Algorithm 1 requires the number of outputs to be less than the number of minimal states. The bongoboard model, which is used as a generic model representing the different environments considered in this paper, has six minimal states, and therefore, Algorithm 1 restricts us to have a maximum of five outputs. This section proposes to derive an output

feedback controller for the generic bongoboard model such that the same controller stabilizes the other models as well.

### A. Optimizing the range of stabilizable wheel radii

As discussed in Sec. III, the bongoboard model is used as the generic model with wheel radii $r_w = 0$ and $r_w = \infty$ corresponding to the two discrete cases of seesaw and flat floor models respectively. The bongoboard model with constant wheel density $\rho_w$ and wheel radius $r_w \in (0, \infty)$ corresponds to a continuum of bongoboard and curved floor models. Since the bongoboard model with constant wheel density and zero or infinite wheel radius results in a degenerate model, a seesaw model is used to represent these two discrete cases.

The user-defined matrices that affect the output-feedback controller design using Algorithm 1 are $Q, R$ and $X$. In this work, the matrices $R$ and $X$ are chosen to be identity matrices, and hence the only tunable matrix is $Q$. This section presents an optimization algorithm that optimizes for the elements of $Q$ matrix such that the resulting output feedback controller stabilizes the seesaw and flat floor models, and also stabilizes the largest family of bongoboard and curved floor models, $i.e.$, the largest range of wheel radii.

In this work, $Q \in \mathbb{R}^{12\times12}$ for the bongoboard model in Sec. III-A is chosen to be a diagonal matrix, with equal weights for the configurations of the left and right legs. Therefore, the matrix $Q \in \mathbb{R}^{12\times12}$ for the bongoboard model is parameterized by eight parameters as follows:

$$Q = diag\big([a_1,a_2,a_3,a_3,a_4,a_4,a_5,a_6,a_7,a_7,a_8,a_8]^T\big), \quad (14)$$

and the matrix $Q_m \in \mathbb{R}^{6\times6}$ corresponding to the minimal system $\{A_m, B_m, C_m\}$ with minimal state transformation $U_m$ is obtained as $Q_m = U_m Q U_m^T$. The other user-defined matrices include $R_m = I_4$ and $X_m = I_6$. With four control inputs and five outputs to feedback, the output feedback control gain $F \in \mathbb{R}^{4\times5}$ is obtained using $OFC(A_m, B_m, C_m, Q_m, R_m, X_m)$ in Algorithm 1.

The problem of finding the universal controller can now be formulated as an optimization problem of finding the eight parameters $\{a_i\}$ of $Q$ in Eq. 14 such that the resulting output feedback controller stabilizes the seesaw and flat floor models, and also stabilizes the largest family of bongoboard and curved floor models, $i.e.$, the largest range of wheel radii. The optimization problem is formulated as follows:

$$\underset{\{a_i\}}{\text{minimize}} \quad J = w_1J_1 + w_2J_2 + w_3J_3 + w_4J_4 + w_5J_5, \quad (15)$$

where, $w_1 - w_5$ are user-defined weights,

$$J_1 = \begin{cases} 1 & \text{when } F \text{ fails on flat floor model} \\ 0 & \text{when } F \text{ stabilizes flat floor model} \end{cases}, \quad (16)$$

$$J_2 = \begin{cases} 1 & \text{when } F \text{ fails on seesaw model} \\ 0 & \text{when } F \text{ stabilizes seesaw model} \end{cases}, \quad (17)$$

$$J_3 = \frac{r_{low}}{r_{min}}, \quad (18)$$

$$J_4 = \frac{r_{max}}{r_{up}}, \quad (19)$$

$$J_5 = ||G^d||_\infty, \quad (20)$$

where $F$ is the output feedback gain derived for the nominal bongoboard model using Algorithm 1 with the chosen $Q$ at each iteration, $r_{low}, r_{up}$ are the lower and upper bounds respectively of the range of stabilizable wheel radii for the bongoboard models, $r_{min}, r_{max}$ are the minimum and maximum bounds respectively of the range of wheel radii for which the output feedback gain $F$ is evaluated, and $G^d$ is the transfer function from the disturbance torque on the board to the outputs of the nominal closed loop system with output feedback gain $F$ given by

$$G^d = \begin{bmatrix} A_m^d & B_m^d \\ C_m^d & 0_{5\times1} \end{bmatrix}, \quad (21)$$

where $\{A_m^d, B_m^d, C_m^d\}$ is the minimal realization of $\{A^d, B^d, C^d\}$ given by

$$\begin{aligned} A^d &= A - BFC \in \mathbb{R}^{12\times12}, \\ B^d &= \begin{bmatrix} 0_{6\times4} \\ N_2 s_d^T \end{bmatrix}\Big|_{q=0} \in \mathbb{R}^{12\times1}, \\ C^d &= C \in \mathbb{R}^{5\times12}, \end{aligned} \quad (22)$$

where $N_2 = M^{-1}(I_6 - N_1\Psi M^{-1})$, $N_1 = \Psi^T(\Psi M^{-1}\Psi^T)^{-1}$, $s_d = [0, 1, 0, 0, 0, 0]$. Here, the input is the disturbance torque to the board, and the outputs are the same as in Eq. 13.

The norm $||G^d||_\infty$ represents the sensitivity of the outputs of the closed loop system in Eq. 22 to the disturbance on the board. Lower the norm, lower is the sensitivity and more robust is the output feedback controller to the bongoboard disturbances. The term $J_5$ in Eq. 20 is used to ensure that the disturbance rejection of the nominal closed loop system is not compromised in an attempt at enlarging the range of stabilizable wheel radii. Large values are chosen for $w_1$ and $w_2$ in order to drive the optimization towards finding output feedback gains that stabilize the seesaw and flat floor models. The $w_3 - w_5$ determine the relative weighting between the lower and upper bounds of the range of stabilizable wheel radii and the disturbance $H_\infty$ norm. The overall optimization algorithm is presented in Algorithm 2. In this work, the optimizer update in Step 10 of Algorithm 2 was performed using the Nelder-Mead simplex method [19].

The range of stabilizable wheel radii in Step 7 of Algorithm 2 is obtained using a bisection algorithm shown in Algorithm 3. This work assumes that the density of the wheel $\rho_w$ remains constant, and hence with changing wheel radii $r_w$, the mass and moment of inertia of the wheel also change and are given by $m_w = \pi r_w^2 \rho_w$ and $I_w = \frac{1}{2}\pi r_w^4 \rho_w$ respectively. In this work, the minimum $r_{min}$ and maximum $r_{max}$ allowable wheel radii for Algorithm 3 are set to 0.001 m and 122.7108 m respectively beyond which the reciprocal of the condition number of the mass/inertia matrix $M(q)$ of the system becomes $< 10^{-12}$, and hence becomes too close to singular. For a sufficiently large wheel radius, the mass and moment of inertia of the wheel are large enough that the wheel doesn't move and the model reduces to the curved floor model. The wheel radii range of [0.001 m, 122.7108 m] is sufficient to evaluate the stabilizable range of an output feedback controller, and any controller that can stabilize this

**Algorithm 2:** Optimizing Output Feedback Gain

**input** : Initial Parameters $\{a_i^0\}$, Matrices $R_m, X_m$
Minimal System $\{A_m, B_m, C_m\}$,
State Transformation $U_m$, Weights $\{w_i\}$,
Nominal Radius $r_{nom}$, Bounds $r_{min}, r_{max}$
**output** : Optimal output feedback gain $F^*$
**function**: $F^*$ = OptimizeOFC($\cdots$)

**begin**
  Initialize parameters of $Q$ and overall cost function $J$
    $\{a_i\} = \{a_i^0\}$, $J = \eta \gg 0$
  **repeat**
    Get new $Q$ and $Q_m$ matrices
      $Q(\{a_i\})$ (Eq. 14), $Q_m = U_m Q U_m^T$
    Get nominal output feedback gain (Algorithm 1)
      $F$ = OFC($A_m, B_m, C_m, Q_m, R_m, X_m$)
    Evaluate stability of flat floor and seesaw models
      $J_1$, $J_2$ (Eq. 16−17)
    Get range of stabilizable wheel radii (Algorithm 3)
      $[r_{low}, r_{up}]$ = StabilizableRadii($F, r_{nom}, r_{min}, r_{max}$)
      $J_3 = \frac{r_{low}}{r_{min}}$, $J_4 = \frac{r_{max}}{r_{up}}$ (Eq. 18−19)
    Get disturbance $H_\infty$-norm for nominal system
      $J_5 = ||G^d||_\infty$ (from Eq. 21)
    Get overall cost function
      $\Delta J = w_1 J_1 + w_2 J_2 + w_3 J_3 + w_4 J_4 + w_5 J_5 - J$
      $J = J + \Delta J$
    Update parameters of $Q$
      $\Delta\{a_i\}$ = OptimizerUpdate($J, \{a_i\}$)
      $\{a_i\} = \{a_i\} + \Delta\{a_i\}$
  **until** $\Delta J < \epsilon_J$ *or* $\Delta\{a_i\} < \epsilon_a$
  Get optimal output feedback gain
    $F^* = F$
**end**

**Algorithm 3:** Find Range of Stabilizable Wheel Radii

**input** : Output Feedback Gain $F$
Nominal Radius $r_{nom}$, Bounds $r_{min}, r_{max}$
**output** : Stabilizable Range $r_{low}, r_{up}$
**function**: $[r_{low}, r_{up}]$ = StabilizableRadii($F, r_{nom}, r_{min}, r_{max}$)

**begin**
  $r_{mid} = r_{nom}$
  **while** $(r_{mid} - r_{min}) > \epsilon_r$ **do**
    Update lower bound
      $r_{low} = \frac{1}{2}(r_{min} + r_{mid})$
    Get new minimal system
      $[A_m, B_m, C_m]$ = MinimalBongoboard($r_{low}$)
    Find unstable closed loop poles
      $p_{unstab} = \{\lambda_i | \lambda_i \in \lambda(A_m - B_m F C_m) \geq 0\}$
    **if** $p_{unstab} \neq \emptyset$ **then**
      $r_{min} = r_{low}$
    **else**
      $r_{mid} = r_{low}$
    **end**
  **end**
  $r_{mid} = r_{nom}$
  **while** $(r_{max} - r_{mid}) > \epsilon_r$ **do**
    Update upper bound
      $r_{up} = \frac{1}{2}(r_{mid} + r_{max})$
    Get new minimal system
      $[A_m, B_m, C_m]$ = MinimalBongoboard($r_{up}$)
    Find unstable closed loop poles
      $p_{unstab} = \{\lambda_i | \lambda_i \in \lambda(A_m - B_m F C_m) \geq 0\}$
    **if** $p_{unstab} \neq \emptyset$ **then**
      $r_{max} = r_{up}$
    **else**
      $r_{mid} = r_{up}$
    **end**
  **end**
**end**

wide family of bongoboards and curved floors, and also the seesaw and flat floor models is considered worthy enough to be called the universal controller.

## V. Performance Comparison and Analysis

This section presents a detailed analysis of the universal controller derived using Algorithm 2, and compares its performance and robustness with other controllers like linear quadratic regulator (LQR) and $H_\infty$ controllers.

### A. Controllers under comparison

*1) Universal Controller:* The optimal output feedback gain $F \in \mathbb{R}^{4\times5}$ obtained using Algorithm 2 for the system with nominal parameters shown in Table I and the output matrix $C \in \mathbb{R}^{5\times12}$ shown in Eq. 13 is given below:

$$F = 10^6 \times \begin{bmatrix} -2.7167 & -1.1894 & 0.9536 & 0.0101 & 0.7685 \\ -2.7167 & -1.1894 & 0.9536 & 0.0101 & 0.7685 \\ 2.7167 & 1.1894 & -0.9536 & -0.0101 & -0.7685 \\ 2.7167 & 1.1894 & -0.9536 & -0.0101 & -0.7685 \end{bmatrix}. \quad (23)$$

In this work, the robot is redundantly actuated and hence, the terms corresponding to hip and ankle torques are equal and opposite to each other.

*2) LQR Controller:* The LQR controller compared here is obtained by optimizing for the elements of its $Q$ matrix using an algorithm similar to Algorithm 2 such that the objective function in Eq. 15 is minimized and the range of stabilizable wheel radii is maximized. However, this algorithm ignored cost functions $J_1$ (Eq. 16) and $J_2$ (Eq. 17) since the state feedback LQR controller for the bongoboard model cannot be used to stabilize flat floor and seesaw models with state spaces of different dimensions. The $R$ matrix here is also chosen to be an identity matrix. Due to insufficient space, the derived LQR gain matrix is not provided here.

*3) $H_\infty$ controller:* The linear, minimal state space equations used for $H_\infty$ control design are as follows:

$$\begin{aligned} \dot{x}_m &= A_m x_m + B_m^d u_d + B_m u, \\ \tilde{y} &= \tilde{C} x_m + \tilde{D} u_d, \\ y_m &= C_m x_m, \end{aligned} \quad (24)$$

where $\{A_m, B_m, C_m\}$ is the minimal realization of the nominal bongoboard model, $B_m^d \in \mathbb{R}^{6\times1}$ is the minimal input transfer matrix corresponding to the disturbance input

$u_d$ on the board as shown in Eq. 22, and

$$\tilde{C} = \begin{bmatrix} \sqrt{U_m Q U_m^T} \\ 0_{4\times 6} \end{bmatrix} \in \mathbb{R}^{10\times 6},$$
$$\tilde{D} = \begin{bmatrix} 0_{6\times 4} \\ \sqrt{R} \end{bmatrix} \in \mathbb{R}^{10\times 4}, \quad (25)$$

where $\sqrt{(\cdot)}$ refers to the Cholesky factor of the corresponding matrix. The $H_\infty$ controller is a state space model with six states, five inputs ($y_m$) and four outputs ($u$), and is designed such that the $H_\infty$ norm of the transfer function from disturbance input $u_d$ to output $\tilde{y}$, *i.e.*, $||T_{\tilde{y}u_d}||_\infty$ is minimized. It can be seen from Eq. 24 and Eq. 25 that the matrix $Q$ affects the output $\tilde{y}$ of the system, which in turn affects the $H_\infty$ controller. Here, similar to the universal and LQR controllers, the elements of the $Q$ matrix are optimized using an algorithm similar to Algorithm 2 such that the objective function in Eq. 15 is minimized.

### B. Universality and Range of Stabilizable Wheel Radii

Tables II compares the performance of the different controllers described in Sec. V-A in stabilizing the flat floor, seesaw, and family of bongoboard and curved floor models. The stabilizability guarantees were derived using linearized dynamics of the respective models. Unlike the full state-feedback LQR controller in Sec. V-A.2, the $H_\infty$ controller in Sec. V-A.3 is an output feedback controller and can be used to stabilize the nominal seesaw and flat floor models. However, the best $H_\infty$ controller derived here was unable to stabilize both these systems as shown in Table II, whereas, the universal controller was capable of successfully stabilizing both the nominal seesaw and flat floor models. For the family of bongoboard and curved floor models, the range of stabilizable wheel radii for the LQR and $H_\infty$ controllers designed for the nominal bongoboard model are evaluated using the bisection algorithm similar to Algorithm 3. Although the $H_\infty$ controller performs significantly better than the LQR controller by stabilizing a wider range of wheel radii, the universal controller performed orders of magnitude better than the best performing $H_\infty$ controller.

Table II clearly shows that the universal controller derived using Algorithm 2 is able to stabilize the entire range of allowable wheel radii, *i.e.*, [0.001 m, 122.7108 m], and is also able to successfully stabilize the planar robot on the nominal seesaw and flat floor models, making it truly an universal controller for the models considered in this paper.

### C. Disturbance Rejection

Table II also lists the disturbance $H_\infty$ norm of the linear closed loop system in Eq. 21 for the different controllers, and it shows that the $H_\infty$ controller performs better than the universal controller. However, while testing the controllers on a nonlinear simulation of the nominal bongoboard model with actuator limits of $\pm$200 Nm, the universal controller was able to handle a larger disturbance (86.7 Nm for 0.1 s) on the board than that of the $H_\infty$ (36.2 Nm for 0.1 s) and LQR (31.1 Nm for 0.1 s) controllers as shown in Table II.

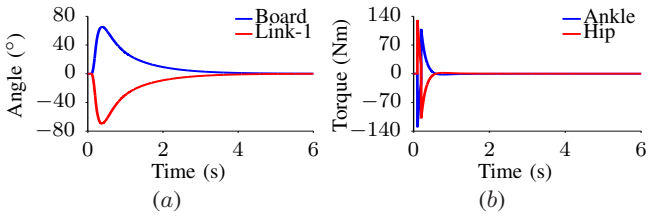


Fig. 3: Universal controller's successful effort in stabilizing a seesaw when subjected to a disturbance of 120 Nm for 0.1 s.

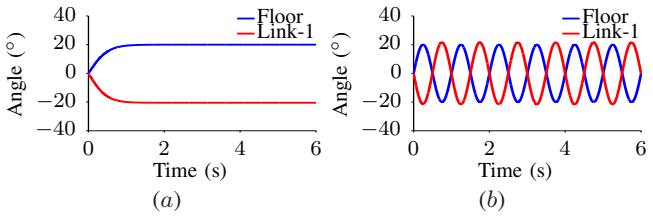


Fig. 4: Universal controller successfully stabilizing on moving floors: ($a$) Tilting to 20° in 2 s, and ($b$) Rocking 20° at 1 Hz.

### D. Robustness to Parameter Uncertainties

Table III shows the range of parameter variations in the nominal bongoboard model that the different controllers can handle. For each parameter except the wheel density $\rho_w$ listed in Table III, while the parameter was varied, the other parameters of the system were maintained at their nominal values. For the wheel density $\rho_w$, however, the mass $m_w$ and moment of inertia $I_w$ varied linearly with $\rho_w$. The stabilizable range of parameter values were obtained using a bisection algorithm similar to Algorithm 3. Table III shows that both the universal and LQR controllers outperform the $H_\infty$ controller by stabilizing a significantly wider range of parameter variations for all parameters. The universal controller is able to stabilize a wider range of parameter variations than the LQR controller for all parameters except the board mass $m_b$ and the link-1 mass $m_1$. Among the values listed in Table III, a stabilizable range written as $(0, \cdot]$ refers to a range whose lower bound is $< 10^{-4}$, and similarly, a stabilizable range written as $[\cdot, \infty)$ refers to a range whose upper bound is $> 10^6$.

## VI. Nonlinear Simulation Results

This section presents the nonlinear simulation results that demonstrate the universality of the universal controller presented in Eq. 23. The constrained nonlinear dynamics of the seesaw and bongoboard models are simulated in MATLAB using $ode15s$ with variable time step, and the actuator inputs are limited to $\pm$200 Nm. The curved floor and flat floor models are derived as special cases of the bongoboard and seesaw models respectively. For all results presented in this paper, the event of the board hitting the floor is ignored.

Figure 3($a$) shows the trajectories of the seesaw's board and the robot's link-1 angles resulting from the universal controller's successful effort in stabilizing the nominal seesaw model when subjected to a disturbance of 120 Nm for 0.1 s. The corresponding ankle and hip torque trajectories are shown in Fig. 3($b$). Similarly, the successful stabilization

TABLE II: Performance comparison with other control approaches: Range of stabilizable wheel radii and Disturbance rejection

| **Control Design** | **Stabilizes Seesaw ($r_w$ = 0 m)** | **Stabilizes on Flat Floor ($r_w = \infty$ m)** | **Stabilizable Bongo Wheel Radii** | | **Disturbance Rejection (Nominal System)** | |
|---|---|---|---|---|---|---|
| | | | **Minimum ($r_{min}$ = 0.001 m)** | **Maximum ($r_{max}$ = 122.7108 m)** | $\|\|G^d\|\|_\infty$ | **Maximum Disturbance Torque for 0.1 s** |
| LQR Control | N/A | N/A | 0.0942 m | 0.1257 m | 0.6676 | 31.2 |
| $H_\infty$ Control | No | No | 0.0363 m | 0.2798 m | 0.2105 | 36.2 |
| **Universal Control** | **Yes** | **Yes** | **0.001 m** | **122.7108 m** | **0.4448** | **86.7** |

TABLE III: Performance comparison with other control approaches: Range of stabilizable system parameters with nominal wheel radius

| **Parameter** | **Symbol** | **Unit** | **Nominal Value** | **Stabilizable Parameter Range** | | |
|---|---|---|---|---|---|---|
| | | | | **LQR Control** | **$H_\infty$ Control** | **Universal Control** |
| Wheel Density | $\rho_w$ | kg·m$^{-3}$ | 200 | (0, $\infty$) | [51.966, 371.030] | **(0, $\infty$)** |
| Wheel Mass | $m_w$ | kg | 6.28 | (0, $\infty$) | (0, 14.342] | **(0, $\infty$)** |
| Wheel Moment of Inertia | $I_w$ | kg·m$^2$ | 0.035 | (0, $\infty$) | (0, 0.112] | **(0, $\infty$)** |
| Board Mass | $m_b$ | kg | 2 | (0, 17.943] | [0.286, 3.812] | **(0, 6.618]** |
| Board Moment of Inertia | $I_b$ | kg·m$^2$ | 0.1067 | (0, 0.553] | [0.013, 0.189] | **(0, 2.848]** |
| Link-1 Mass | $m_1$ | kg | 15 | [11.176, 62.696] | [13.360, 17.106] | **[4.399, 23.889]** |
| Link-1 Moment of Inertia | $I_1$ | kg·m$^2$ | 1 | (0, 2.104] | (0, 1.461] | **(0, 4.426]** |
| Link-1 Length | $l_1$ | m | 1 | [0.8, 1.042] | [0.941, 1.038] | **[0.778, 2.283]** |
| Link-2 Half Mass | $m_2$ | kg | 15 | [12.493, 18.052] | [8.405, 16.609] | **[10.194, 31.391]** |
| Link-2 Half Moment of Inertia | $I_2$ | kg·m$^2$ | 2 | [1.591, 2.223] | [1.953, 2.041] | **[0.986, 3.370]** |
| Link-2 Half Length | $l_2$ | m | 0.1 | (0, 0.157] | [0.079, 0.117] | **(0.055, $\infty$)** |

of the planar bipedal robot on tilting and rocking floors are demonstrated in Fig. 4($a$) and Fig. 4($b$) respectively.

Figure 5($a$1) shows the wheel position trajectory of a bongoboard model with wheel radius $r_w$ = 0.01 m controlled using the universal controller when subjected to a disturbance torque of 6.9 Nm for 0.1 s on the board. The resulting global board angle and link-1 angle trajectories are shown in Fig. 5($a$2), and the corresponding equal and opposite ankle and hip torque trajectories are shown in Fig. 5($a$3). Figures. 5($b$)−5($e$) show similar plots for bongoboard models with radii $r_w$ = 0.05 m to $r_w$ = 0.5 m when subjected to different disturbance torques on the board. More successful simulation results for bongoboard models with wheel radii ranging from 1 m to 100 m when subjected to different disturbance torques on the board are shown in Fig. 6. The plots shown here are for the maximum disturbance torques that the universal controller can successfully reject for the different wheel radii, and one can observe the torque trajectories saturating in the plots in Fig. 5($d$3)−6($d$2). However, input saturations do not result for smaller disturbance torques.

The wheel position trajectories are ignored in Fig. 6 since the wheel barely moves because of the large mass and moment of inertia of the wheel with increasing wheel radii. For wheel radii $r_w > 2$ m, the mass and moment of

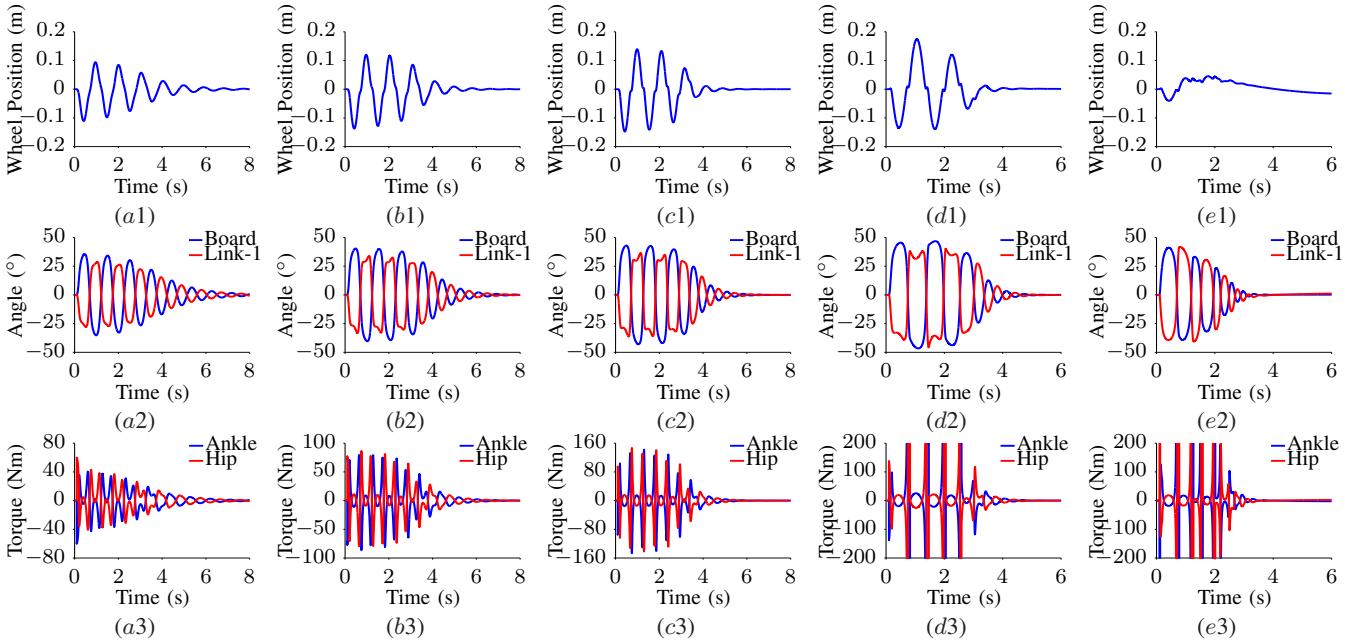


($a$) $r_w = 0.01$ m ($b$) $r_w = 0.05$ m ($c$) $r_w = 0.1$ m ($d$) $r_w = 0.2$ m ($e$) $r_w = 0.5$ m

Fig. 5: Universal controller's successful effort in stabilizing bongoboards with different wheel radii when subjected to the following board disturbances for 0.1 s: ($a$) 6.9 Nm, ($b$) 40 Nm, ($c$) 86.7 Nm, ($d$) 186.3 Nm, and ($e$) 353.4 Nm.

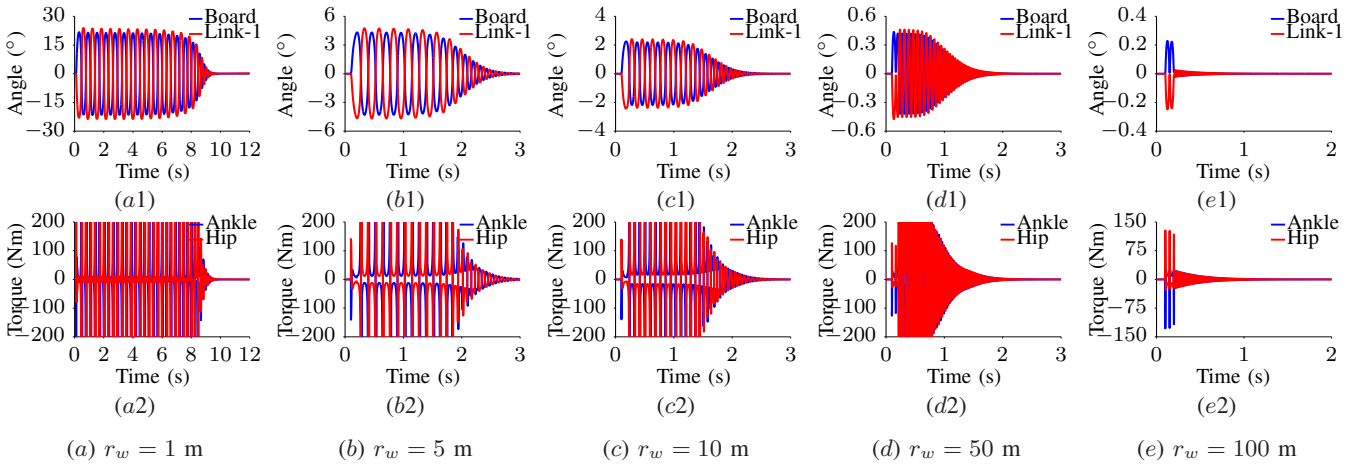


(a) $r_w = 1$ m (b) $r_w = 5$ m (c) $r_w = 10$ m (d) $r_w = 50$ m (e) $r_w = 100$ m

Fig. 6: Universal controller's successful effort in stabilizing bongoboards with different wheel radii when subjected to the following board disturbances for 0.1 s: (a) 246.3 Nm, (b) 131.5 Nm, (c) 129.6 Nm, (d) 119.5 Nm, and (e) 123.6 Nm.

inertia of the wheel are large enough, *i.e.*, $m_w > 2513.3$ kg, $I_w > 5026.5$ kg·$m^2$, that the wheel doesn't move ($< 10^{-3}$ m) and hence, the system reduces to the curved floor case. Moreover, with wheel radius $r_w > 20$ m, the surface of contact of the bongoboard with the wheel is flat and hence, the system reduces to the flat floor case.

Figures 3−6 verify in simulation that the universal controller in Eq. 23 derived using Algorithm 2 can indeed successfully stabilize the nonlinear dynamics of seesaw, flat floor, and family of bongoboard and curved floor models as demonstrated using their linearized dynamics in Table II. Thus, the universal controller presented in this paper is truly universal in stabilizing the family of dynamic, unstable environments considered in this paper.

## VII. Conclusions and Future Work

Output feedback control was proposed as an approach to design a single universal controller that stabilized planar bipedal robots in different dynamic environments with state spaces of different dimensions, and an algorithm that optimizes output feedback controllers to maximize the range of stabilizable systems was also presented. A first of its kind universal balancing controller that stabilizes planar bipedal robots in dynamic, unstable environments like seesaw and bongoboards and also in static environments like flat and curved floors was derived. Moreover, it was shown that the universal controller presented in this paper performed significantly better than the similarly derived LQR and $H_\infty$ controllers in both disturbance rejection and also in robustness to parameter uncertainties. Several nonlinear simulation results were presented to demonstrate the robustness and universality of the derived universal controller.

As part of future work, the derived universal controller needs to be experimentally validated. In this work, the outputs needed to stabilize the system were hand-picked using designer's intuition. Automatic approaches to determine these outputs is an interesting future direction to explore. The motion capture data of humans balancing in dynamic, unstable environments like seesaw and bongoboards can be potentially used to obtain these outputs.

## References


[1] S. Hyon, J. G. Hale, and G. Cheng, "Full-body compliant human-humanoid interaction: Balancing in the presence of unknown external forces," *IEEE Trans. Robotics*, vol. 23, no. 5, pp. 884–898, 2007.

[2] C. Ott, M. A. Roa, and G. Hirzinger, "Posture and balance control for biped robots based on contact force optimization," in *Proc. IEEE Int'l Conf. on Humanoid Robots*, 2011, pp. 26–33.

[3] J. Pratt, J. Carff, S. Drakunov, and A. Goswami, "Capture point: A step toward humanoid push recovery," in *Proc. IEEE-RAS Int'l Conf. on Humanoid Robots*, 2006, pp. 200–207.

[4] B. Stephens, "Humanoid push recovery," in *Proc. IEEE Int'l Conf. on Humanoid Robots*, 2007, pp. 589–595.

[5] S. Kajita, F. Kanehiro, K. Kaneko, K. Fujiwara, K. Harada, K. Yokoi, and H. Hirukawa, "Biped walking pattern generation by using preview control of zero-moment point," in *Proc. IEEE Int'l Conf. on Robotics and Automation*, 2003, pp. 1620–1626.

[6] K. Byl and R. Tedrake, "Metastable walking machines," *Int'l Journal of Robotics Research*, vol. 28, no. 8, pp. 1040–1064, 2009.

[7] C. E. Bauby and A. D. Kuo, "Active control of lateral balance in human walking," *Journal of Biomechanics*, vol. 33, no. 11, pp. 1433–1440, 2000.

[8] P. Huber and R. Kleindl, "A case study on balance recovery in slacklining," in *Proc. Int'l Conf. on Biomechanics in Sports*, 2010.

[9] P. Paoletti and L. Mahadevan, "Balancing on tightropes and slacklines," *J. R. Soc. Interface*, vol. 9, no. 74, pp. 2097–2108, 2012.

[10] S.-H. Lee and A. Goswami, "A momentum-based balance controller for humanoid robots on non-level and non-stationary ground," *Autonomous Robots*, vol. 33, no. 4, pp. 399–414, 2012.

[11] Y. Zheng and K. Yamane, "Ball walker: a case study of humanoid robot locomotion in non-stationary environments," in *Proc. IEEE Int'l Conf. on Robotics and Automation*, 2011, pp. 2021–2028.

[12] S. O. Anderson, J. K. Hodgins, and C. G. Atkeson, "Approximate policy transfer applied to simulated bongo board balance," in *Proc. IEEE Int'l Conf. on Humanoid Robots*, 2007, pp. 490–495.

[13] S. O. Anderson and J. K. Hodgins, "Adaptive torque-based control of a humanoid robot on an unstable platform," in *Proc. IEEE Int'l Conf. on Humanoid Robots*, 2010, pp. 511–517.

[14] A. Trofino-Neto, "Stabilization via static output feedback," *IEEE Trans. on Automatic Control*, vol. 38, no. 5, pp. 764–765, 1993.

[15] V. L. Syrmos, C. T. Abdallah, P. Dorato, and K. Grigoriadis, "Static output feedback - a survey," *Automatica*, vol. 33, no. 2, pp. 125–137, 1997.

[16] J. Yu, "A convergent algorithm for computing stabilizing static output feedback gains," *IEEE Trans. on Automatic Control*, vol. 49, no. 12, pp. 2271–2275, 2004.

[17] M. M. Rosenbrock, *State-Space and Multivariable Theory*. John Wiley, 1970.

[18] Y.-L. Tsai, T.-T. Hu, H. Bae, and P. Chou, "EcoIMU: A dual triaxial-accelerometer inertial measurement unit for wearable applications," in *Proc. Int'l Conf. on Body Sensor Networks*, 2010.

[19] J. Nelder and R. Mead, "A simplex method for function minimization," *The Computer Journal*, vol. 7, pp. 308–313, 1964.